

GAFD Special issue on “Physics and Algorithms of the Pencil Code”

*Convergence properties of detonation simulations*CHENGENG QIAN^a, CHENG WANG^a, JIANNAN LIU^b, AXEL BRANDENBURG^{c,d,e*},
NILS E. L. HAUGEN^f, and MIKHAIL A. LIBERMAN^c^aState Key Laboratory of Explosion Science and Technology, Beijing Institute of Technology,
Beijing, 100081, China^bCollege of Mining Engineering, Taiyuan University of Technology, Taiyuan 030024, China^cNordita, KTH Royal Institute of Technology and Stockholm University,
Roslagstullsbacken 23, SE-10691 Stockholm, Sweden^dDepartment of Astronomy, Stockholm University, SE-10691 Stockholm, Sweden^eJILA and Laboratory for Atmospheric and Space Physics, University of Colorado,
Boulder, CO 80303, USA^fSINTEF Energy Research, 7465 Trondheim, Norway*(February 12, 2019, Revision: 1.78)*

We present a high-resolution convergence study of detonation initiated by a temperature gradient in a stoichiometric hydrogen–oxygen mixture using the PENCIL CODE. With Mach numbers reaching 10–30, a certain amount of shock viscosity is needed to remove or reduce numerical pressure oscillations on the grid scale at the position of the shock. Detonation is found to occur for intermediate values of the shock viscosity parameter. At fixed values of this parameter, the numerical error associated with those small wiggles in the pressure profile is found to decrease with decreasing mesh width δx like $\delta x^{-1.4}$.

Keywords: Combustion; numerical methods; detonation; shock waves; chemical reaction.

1. Introduction

Detonation can be produced by the coupling of a spontaneous reaction wave, which propagates along an initial temperature gradient, with a pressure wave (Zeldovich *et al.* 1970, Zeldovich 1980). This process is governed by the time-dependent compressible reactive Navier-Stokes equations. Its direct numerical simulation (DNS) is an intricate problem that is of fundamental importance for understanding the ignition of different combustion modes caused by a transient thermal energy deposition localised in a finite volume of reactive gas (Lieberman *et al.* 2012). High resolution methods are necessary to resolve the broad range of length scales. It is also well-known that problems involving strong shocks, such as in the final stage of the deflagration to detonation transition (DDT), require the use of shock-capturing techniques to eliminate or reduce spurious oscillations near discontinuities. One of the widely used approaches is the use of weighted essentially non-oscillating (WENO) finite differences (Jiang and Shu 1996), which is an improvement upon the essentially non-oscillating (ENO) scheme. The main idea of the WENO scheme is to use a convex combination of all the candidate stencils rather than the smoothest candidate stencil to achieve a higher order accuracy than the ENO scheme, while maintaining the essentially non-oscillating property near discontinuities. There are also other methods such as the Total Variation Diminishing (TVD) method or the Artificial Compression

*Email: brandenb@nordita.org

Method (ACM) switch (Lo *et al.* 2007).

Yet another approach to avoid wiggles in the numerical solution is to add a shock-capturing viscosity. However, one must be cautious when using such a shock-capturing viscosity, since its properties are problem-dependent. The shock-capturing viscosity will fail to eliminate oscillations if it is too small. Since the gaseous combustion process is highly sensitive to the resolution of the reaction zone, using too large shock-capturing viscosity can lead to an artificial coupling of the leading pressure wave and the flame front. Thus, it is essential to determine the proper shock-capturing viscosity when using the PENCIL CODE to simulate problems involving the onset of detonation.

The test problem examined in this paper is the hot spot problem, which is a chemically exothermic reactive mixture with a nonuniform distribution of temperature. According to the theory developed by Zeldovich *et al.* (1970) and Zeldovich (1980), the gradient of induction time associated with temperature (or concentration) gradients may be ultimately responsible for the detonation initiation. A similar concept of shock-wave amplification by coherent energy release (SWACER) was introduced later by Lee and Moen (1980). The basic idea is that a spontaneous reaction wave can propagate through a reactive gas mixture if there is a spatial gradient in the chemical induction time τ_{ind} . The spontaneous reaction wave is ignited first at the location of minimum induction (ignition delay) time τ_{ind} and then spreads by spontaneous ignition over neighbouring locations where the temperature is lower and τ_{ind} is correspondingly longer. The velocity of the spontaneous reaction wave is analogous to a phase velocity. It cannot be smaller than the velocity of deflagration, but is not limited from above, and depends on the steepness of the temperature gradient and the temperature derivative of the induction time. The proposed mechanism of detonation initiated by the temperature gradient suggests that the formation of an induction time gradient produces a spatial time sequence of energy release, which then produces a compression wave that gradually amplifies into a shock wave. Coupling of the spontaneous reaction and pressure waves can cause shock wave amplification by coherent energy release and can finally result in the formation of a detonation wave. This requires a certain synchrony between the progress of the shock and the sequential release of chemical energy by successive reactions along of the temperature gradient.

The first demonstration of the ignition of a detonation wave by a temperature gradient was by Zeldovich *et al.* (1970). Although this earliest numerical simulations had a low resolution, the authors demonstrated successfully that sufficiently shallow gradients produce detonation, while for steeper gradients the reaction wave and the shock failed to couple together. In subsequent studies, Zeldovich *et al.* (1988), He and Clavin (1992), He (1996), Khokhlov *et al.* (1997), Bartenev and Gelfand (2000), and Kurtz and Regele (2014) have employed a one-step chemical model to investigate regimes of detonation ignition by an initial temperature gradient. However, the one-step model or other simplified chemical models do not predict correctly the induction time for the combustion process involving a large set of chain-branching reactions. Liberman *et al.* (2011, 2012) studied different modes of combustion produced by the initial temperature gradient in stoichiometric hydrogen–oxygen and hydrogen–air mixtures ignited by a temperature gradient using detailed chemical models and compared the results with those obtained with a one-step chemical model. In particular, it was shown that the minimal slope of the temperature gradient required for triggering detonation and other combustion modes obtained in simulations with simplified chemical models, for example a one-step model, is orders of magnitude smaller than those obtained in simulations with a detailed chemical model. Wang *et al.* (2018) and Liberman *et al.* (2018) studied the influence of the chemical reaction model on detonation ignited by a temperature gradient for hydrogen–air and methane–air mixtures. They concluded that the one-step model and other simplified models usually cannot describe correctly the ignition processes. Thus, using simplified chemical kinetics for understanding the mechanisms of DDT must be considered with great caution.

The aim of this paper is to study the convergence of detonations simulation using the

PENCIL CODE. The paper is organised as follows. In section 2, the governing equations are presented and the setup of the hot spot problem is described. Section 3 presents a convergence study of the pressure profiles obtained using the PENCIL CODE. The dependence on the shock viscosity is also investigated in this section. In section 4, we conclude by summarising our main findings.

2. The model

2.1. The basic equations

The set of equations for modelling combustion was implemented into the PENCIL CODE by Babkovskaia *et al.* (2011). Considering a mixture of N_s species undergoing N_r reactions, we solve the continuity equation for the total density ρ ,

$$\frac{D \ln \rho}{Dt} = -\nabla \cdot \mathbf{U}, \quad (1)$$

the momentum equation for the velocity \mathbf{U} ,

$$\frac{D\mathbf{U}}{Dt} = -\frac{1}{\rho}\nabla p + \frac{2}{\rho}\nabla \cdot \boldsymbol{\tau}, \quad (2)$$

the energy equation for the temperature T ,

$$c_v \frac{D \ln T}{Dt} = \sum_k^{N_s} \frac{DY_k}{Dt} \left(\frac{R}{W_k} - \frac{h_k}{T} \right) - \frac{R}{W} \nabla \cdot \mathbf{U} + \frac{\boldsymbol{\tau} : \nabla \mathbf{U}}{\rho T} - \frac{\nabla \cdot \mathbf{q}}{\rho T}, \quad (3)$$

and the equation for the mass fraction of the k th species Y_k in the form

$$\rho \frac{DY_k}{Dt} = -\nabla \cdot \mathbf{J}_k + \dot{\omega}_k, \quad (4)$$

where $D/Dt = \partial/\partial t + \mathbf{U} \cdot \nabla$ is the advective derivative and $\tau_{ij} = 2\rho\nu S_{ij} + \rho\zeta\delta_{ij}\nabla \cdot \mathbf{U}$ are the components of the stress tensor with $S_{ij} = \frac{1}{2}(\partial U_i/\partial x_j + \partial U_j/\partial x_i) - \frac{1}{3}\delta_{ij}\nabla \cdot \mathbf{U}$ being the components of the traceless rate-of-strain tensor, ν is the kinematic viscosity, ζ is the bulk viscosity, $\dot{\omega}$ is the reaction rate and subscript k refers to species number k . The pressure is given by the equation of state,

$$p = \rho T \frac{R}{W} = \rho T R \sum_{k=1}^{N_s} \left(\frac{Y_k}{W_k} \right), \quad (5)$$

where R , W , and W_k are the universal gas constant, the molecular weight of species k , and the mean molecular weight of the mixture, respectively. The viscosity of species k is given by Coffee and Heimerl (1981) as

$$\mu_k = \frac{5}{16} \frac{\sqrt{\pi k_B T m_k}}{\pi \sigma_k^2 \Omega_k^{(2,2)*}}, \quad (6)$$

where σ_k is the Lennard-Jones collision diameter, k_B is the Boltzmann constant, m_k is the mass of the molecule, and $\Omega_k^{(2,2)*}$ is the collision integral (see Mourits and Rummens 1977). Then, the viscosity of the mixture, $\mu = \rho\nu_{\text{mix}}$, is given by (Wilke 1950)

$$\mu = \sum_{k=1}^{N_s} \left(X_k \mu_k \left/ \sum_{j=1}^{N_s} X_j \Phi_{kj} \right. \right). \quad (7)$$

Here, X_k is the mole fraction of species k and Φ_{kj} is given by

$$\Phi_{kj} = \frac{1}{\sqrt{8}} \left(1 + \frac{W_k}{W_j}\right)^{-1/2} \left[1 + \left(\frac{\mu_k}{\mu_j}\right)^{1/2} \left(\frac{W_j}{W_k}\right)^{1/4}\right]^2. \quad (8)$$

The heat flux \mathbf{q} is given by

$$\mathbf{q} = \sum_{k=1}^{N_s} h_k \mathbf{J}_k - \lambda \nabla T. \quad (9)$$

Here, $\mathbf{J}_k = \rho Y_k \mathbf{V}_k$ is the diffusive flux. Fick's law is employed to calculate the diffusion velocity \mathbf{V}_k as (Poinsot and Veynante 2005)

$$\mathbf{V}_k = -\frac{D_k}{X_k} \nabla X_k, \quad (10)$$

where the diffusion coefficient for species k is expressed as

$$D_k = \frac{1 - Y_k}{\sum_{j \neq k}^{N_s} X_j / D_{jk}}, \quad (11)$$

and the binary diffusion coefficient is given by

$$D_{jk} = \frac{3}{16} \frac{\sqrt{2\pi k_B^3 T^3 / m_{jk}}}{p\pi\sigma_{jk}^2 \Omega_{jk}^{(1,1)*}}, \quad (12)$$

where $\Omega_{jk}^{(1,1)*}$, σ_{jk} , and m_{jk} are given by Evlampiev (2007).

The thermal conductivity for pure species k is expressed as

$$\lambda_k = \frac{\mu_k}{W_k} (f_{\text{trans}} \cdot C_{v,\text{trans}} + f_{\text{rot}} \cdot C_{v,\text{rot}} + f_{\text{vib}} \cdot C_{v,\text{vib}}), \quad (13)$$

and the thermal conductivity of the mixture follows an empirical law. The specific heat $c_{p,k}$ and specific enthalpy h_k of species k are calculated by using tabulated polynomials used in rocket science by the National Aeronautics and Space Administration (NASA) and are known as NASA polynomials. We use here the coefficients from Kéromnès *et al.* (2013).

The expression for the reaction rate is (Poinsot and Veynante 2005)

$$\dot{\omega}_k = W_k \sum_{s=1}^{N_r} (\nu''_{ks} - \nu'_{ks}) \left[k_{f,s} \prod_{j=1}^{N_s} \left(\frac{\rho_j}{W_j}\right)^{\nu'_{js}} - k_{r,s} \prod_{j=1}^{N_s} \left(\frac{\rho_j}{W_j}\right)^{\nu''_{js}} \right], \quad (14)$$

where ρ_k is the density of species k . Furthermore, ν'_{ks} and ν''_{ks} are the stoichiometric coefficients of species k of reaction s on the reactant and product sides, respectively. Furthermore, $k_{f,s}$ is the forward rate of reaction s , which is given by

$$k_{f,s} = B_s T^{\alpha_s} \exp(-E_s/RT), \quad (15)$$

where B_s is a pre-exponential factor, α_s is the temperature exponent, and E_s is the activation energy. These are all empirical coefficients that are given by the kinetic mechanism. The backward rate of reaction s is calculated from the forward rates through the equilibrium constant

$$k_{r,s} = k_{f,s} / k_{c,s}, \quad (16)$$

where $k_{c,s} = (p_0/RT)^{\sum_{k=1}^{N_s} (\nu''_{ks} - \nu'_{ks})} \exp(\Delta S_s/R - \Delta H_s/RT)$. Here $p_0 = 1$ bar, ΔS_s and ΔH_s are entropy and enthalpy changes for reaction s . The detailed chemical mechanism chosen to simulate the hot spot problem is the mechanism developed by Kéromnès *et al.* (2013),

which includes $N_r = 19$ reactions and $N_s = 8$ species. The induction time of this mechanism, which is one of the important parameters for the simulation, has been validated by extensive experiments and simulations at pressure from 1 to 70 bar, over a temperature range of 914 K to 2200 K.

The shock viscosity of von Neumann and Richtmyer (1950) is applied as a bulk viscosity,

$$\zeta = C_{\text{shock}} \delta x^2 \langle -\nabla \cdot \mathbf{U} \rangle_+, \quad (17)$$

and is required to eliminate wiggles in the numerical solution. Here, $\langle \dots \rangle_+$ denotes a running five point average over all positive arguments, corresponding to a compression.

2.2. Setup of the problem

We consider an unburned gas mixture under uniform initial conditions except for the aforementioned linear temperature gradient. The initial conditions at $t = 0$ are constant pressure and zero velocity of the unburned mixture. On the left boundary at $x = 0$, we assume a reflecting wall, where $U_x(x = 0, t) = 0$ and the initial temperature, $T(x = 0) = T^*$ exceeds the ignition threshold value. Thus, the initial conditions are as follows:

$$\begin{aligned} T(x, 0) &= \begin{cases} T^* - (T^* - T_0) x/L, & 0 \leq x \leq L, \\ T_0 & x > L, \end{cases} \\ p(x, 0) &= p_0, \\ \mathbf{U}(x, 0) &= \mathbf{0}. \end{aligned} \quad (18)$$

According to the Zeldovich gradient mechanism, the reactions begin at the temperature maximum, T^* , and then propagate along the temperature gradient due to spontaneous auto-ignition of the mixture. The velocity of the spontaneous reaction wave,

$$U_{\text{sp}} = \frac{dx}{d\tau_{\text{ind}}} = \left(\frac{d\tau_{\text{ind}}}{dT} \right)^{-1} \left(\frac{dT}{dx} \right)^{-1} \quad (19)$$

depends on $d\tau_{\text{ind}}/dT$ and the steepness of the temperature gradient. It could be larger than that of the pressure wave, if the temperature gradient is sufficiently shallow. Then, the coupling between the spontaneous reaction wave with the shock wave, along with the coherent energy release in the reaction, cause shock wave amplification and the transition into a detonation wave. Since we only consider the process of detonation initiation, the parameters in equation (18) are chosen as follows:

$$T^* = 1500 \text{ K}, \quad T_0 = 300 \text{ K}, \quad L = 8 \text{ cm}, \quad p_0 = 1 \text{ bar}. \quad (20)$$

This set of parameters was also used by Liberman *et al.* (2012) to produce a steady detonation wave in a stoichiometric hydrogen–oxygen mixture.

3. Results

3.1. General remarks regarding the transition to detonation (TD)

In the absence of shock viscosity, or when the shock viscosity is too small, small-scale oscillations on the grid scale (wiggles) occur. Such a solution cannot be numerically reliable and must be discarded. When we add shock viscosity, the wiggles become weaker. However, when the shock viscosity is too large, TD is no longer possible. Thus, to pose a meaningful convergence test, we decided to fix the value of C_{shock} to a relatively small value of 0.8 and then increase the resolution. This means that the shock viscosity continuously decreases with increasing resolution until it becomes negligible.

Table 1. Summary of the fit parameters at $t = 42 \mu\text{s}$; x_0 is in cm, p_0 and p_1 are in bar, p'_1 is in $\text{bar } \mu\text{m}^{-1}$, L_1 and L_2 are in μm , and δt_{min} in ps. Runs (a)–(d) have $C_{\text{shock}} = 0.8$ and run (e) has $C_{\text{shock}} = 0.2$.

	δx	x_0	p_1	p'_1	L_1	L_2	N_x	N_t	δt_{min}
(a)	1.993	9.37498	35.00	0.2200	2.56	0.36	50,176	392,000	42
(b)	0.997	9.44825	31.20	0.0546	1.21	0.30	100,352	1,266,600	24
(c)	0.498	9.44390	33.21	0.0535	0.442	0.0587	200,704	2,826,300	12
(d)	0.199	9.27530	35.78	0.1128	0.1145	0.0157	501,760	14,603,000	2.5
(e)	0.199	9.46444	28.70	0.0300	0.4069	0.1719	501,760	14,255,800	2.5

3.2. The pressure wave at increasing resolution

With each doubling of the number of mesh points, the total shock viscosity integrated over the width of the shock decreases by a factor of four. In addition, there is the time-dependent molecular viscosity profile which is independent of the mesh resolution. Thus, we expect that in the limit of infinite resolution, which yields a vanishing shock viscosity, the wiggles of the tip of the pressure profile should disappear. To test this assertion, and to study the corresponding convergence property of the code, we perform four simulations with mesh resolutions between $\delta x = 2 \mu\text{m}$ and $0.2 \mu\text{m}$ using $C_{\text{shock}} = 0.8$; see table 1. The corresponding pressure profiles are shown in figure 1 for the four cases (a)–(d). The insets in each panel show the corresponding pressure profile in the proximity of the peak.

It is evident that the wiggles decrease as we increase the resolution. In addition, the pressure profiles change slightly with resolution. To characterise these changes, we determine a fit to the pressure peak of the form

$$p_{\text{fit}}(x, t_*) = p_0 + [p_1 + (x - x_0) p'_1] \Theta(x_0 - x), \quad (21)$$

where $\Theta(x)$ is the Heaviside step function ($= 1$ for $x > 0$ and zero otherwise), x_0 is the position of the peak at the last time t_* , p_0 is the atmospheric background pressure ahead of the peak, p_1 is the pressure increase relative to p_0 just behind the peak, and p'_1 is the slope of the pressure profile to the left of the peak, i.e., in the wake of the detonation wave. In all cases, the pressure ahead of the peak is $p_0 = 1.013 \times 10^6 \text{ dyn cm}^{-2}$, which does not need to be fitted. The remaining three parameters are given in table 1, where the pressure is given in bar ($1 \text{ bar} = 10^6 \text{ dyn cm}^{-2}$).

Note that between the runs with $\delta x = 1 \mu\text{m}$ and $0.5 \mu\text{m}$, the front speeds (or front positions x_0) agree within 0.05%, but for the run with $\delta x = 0.2 \mu\text{m}$, the front speed has decreased by nearly 2%. The reason for this apparent loss of accuracy is not fully identified, although it is clear that smaller values of C_{shock} lead again to larger front speeds; see run (e) in table 1. It is therefore possible that at this high resolution, the value $C_{\text{shock}} = 0.8$ is already too large and that a smaller value, for example around 0.6, could be more reasonable. We should also point out that we have used a relatively optimistic choice of the viscous time step (we chose $\delta t \nu_{\text{max}} / \delta x^2 = 0.4$ instead of the more conservative value of 0.25 that is recommended in the manual to the PENCIL CODE). However, comparisons with the smaller value did not indicate any differences in the front speed. The fact that the viscous time step enters in this highest resolution run, but not in the others, is related to the extremely small mesh size in this case. This makes the time step constraint from the relatively large molecular viscosity near $x = 0$ very severe. Note also that in this run, waves appear in the wake of the pressure field behind the peak after $t = 36 \mu\text{s}$. These also seem to be spurious and are not found when C_{shock} is smaller.

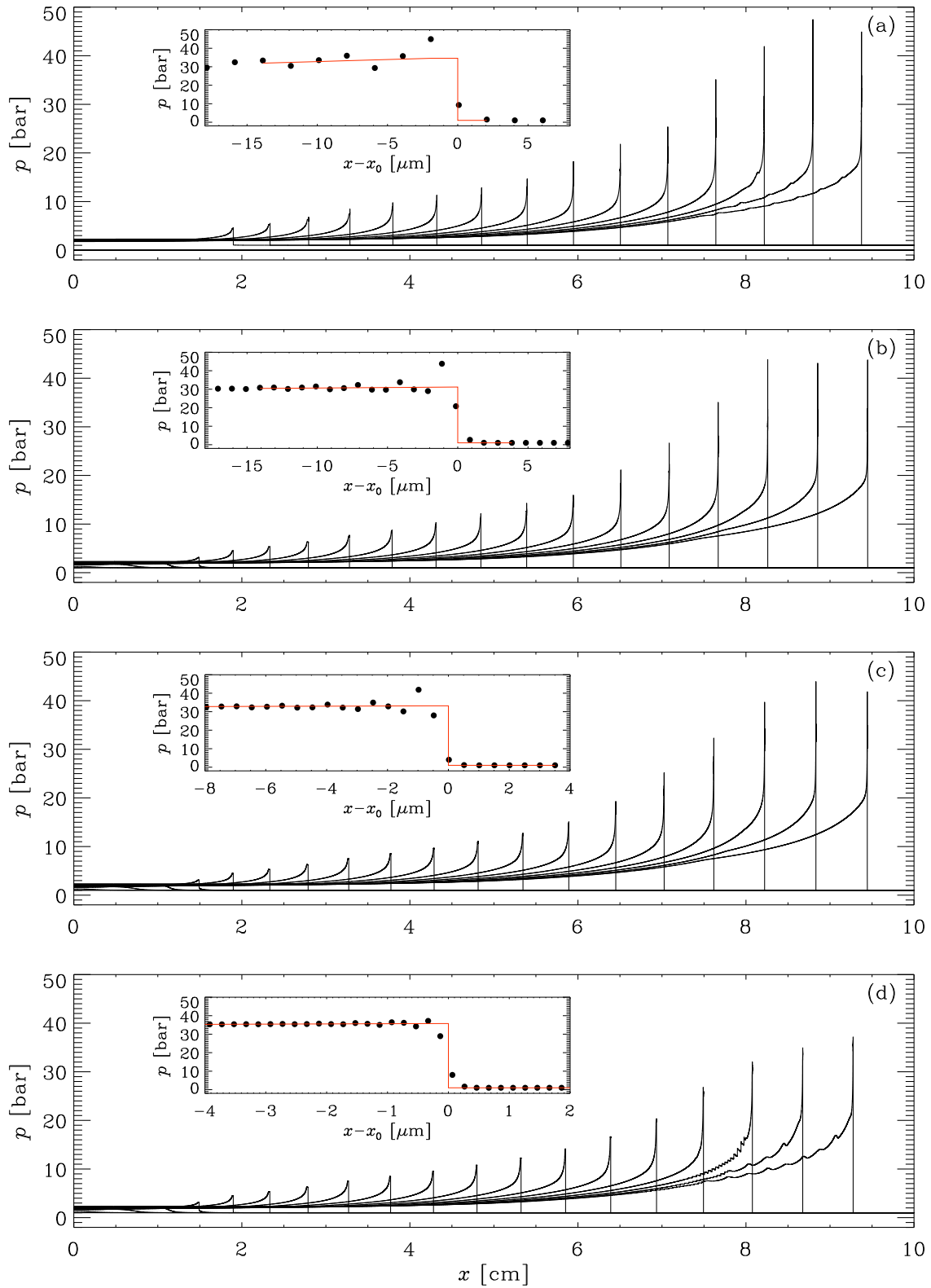
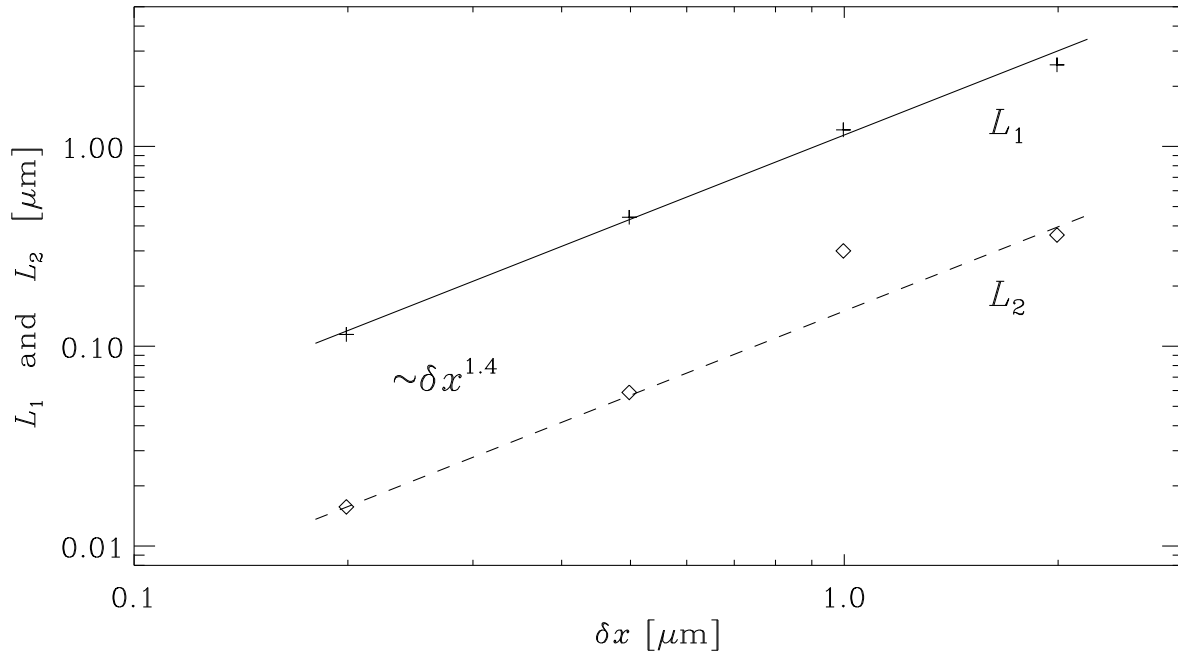


Figure 1. Pressure profiles for (a) $\delta x = 2 \mu\text{m}$, (b) $1 \mu\text{m}$, (c) $0.5 \mu\text{m}$, and (d) $0.2 \mu\text{m}$ in regular time intervals from $t = 2 \mu\text{s}$ to $42 \mu\text{s}$. The insets show the pressure peak at the last time, indicated by filled symbols, where the red line shows the fit in the proximity of the pressure peak. Note that the x range varies.

Figure 2. Convergence of L_1 and L_2 with δx .

Next, to characterise the convergence, we use the L_1 and L_2 norms defined here as follows:

$$L_1 = \int_{x_1}^{x_2} |p(x, t_*) - p_{\text{fit}}(x, t_*)| dx / (p_0 + p_1), \quad (22)$$

$$L_2 = \int_{x_1}^{x_2} |p(x, t_*) - p_{\text{fit}}(x, t_*)|^2 dx / (p_0 + p_1)^2. \quad (23)$$

Both have the dimension of a length. These values are also given in table 1. Figure 2 shows that L_1 and L_2 decrease with resolution like $\delta x^{1.4}$.

In figure 3 we compare the molecular viscosity profile at the last time with the corresponding shock viscosity for the three highest resolutions shown in figures 1(b)–(d). The overall profile of the molecular viscosity is the same in all three cases and varies significantly from $\sim 10 \text{ cm}^2 \text{ s}^{-1}$ at $x = 0$ to $\sim 0.3 \text{ cm}^2 \text{ s}^{-1}$ at and ahead of the shock. However, the peak of the shock viscosity decreases from $\sim 10 \text{ cm}^2 \text{ s}^{-1}$ in figure 1(b) by about a factor of five to $\sim 1.8 \text{ cm}^2 \text{ s}^{-1}$ in figure 1(d). In addition, the width of the shock viscosity profile also decreases by about a factor of five, so the integrated effect of the shock viscosity diminishes by a factor of about 25, as expected from equation (17). Note that for the highest resolution, the shock viscosity makes up a small contribution compared to the We emphasise that the maximum of the molecular viscosity ($\sim 10 \text{ cm}^2 \text{ s}^{-1}$ at $x = 0$) is much larger than the maximum of the shock viscosity ($\sim 1.8 \text{ cm}^2 \text{ s}^{-1}$ at $x = 9.4 \text{ cm}$, although at this point the molecular value is only $\sim 0.3 \text{ cm}^2 \text{ s}^{-1}$); compare figures 3(a) and 3(d). This means that at late times, when ν has become large far in the wake of the shock, an enormous amount of time is spent because the viscous time step is then so short. This is also evident from table 1, where we see that the total number of time steps has increased by a factor of over five as the resolution was increased by only a factor of 2.5.

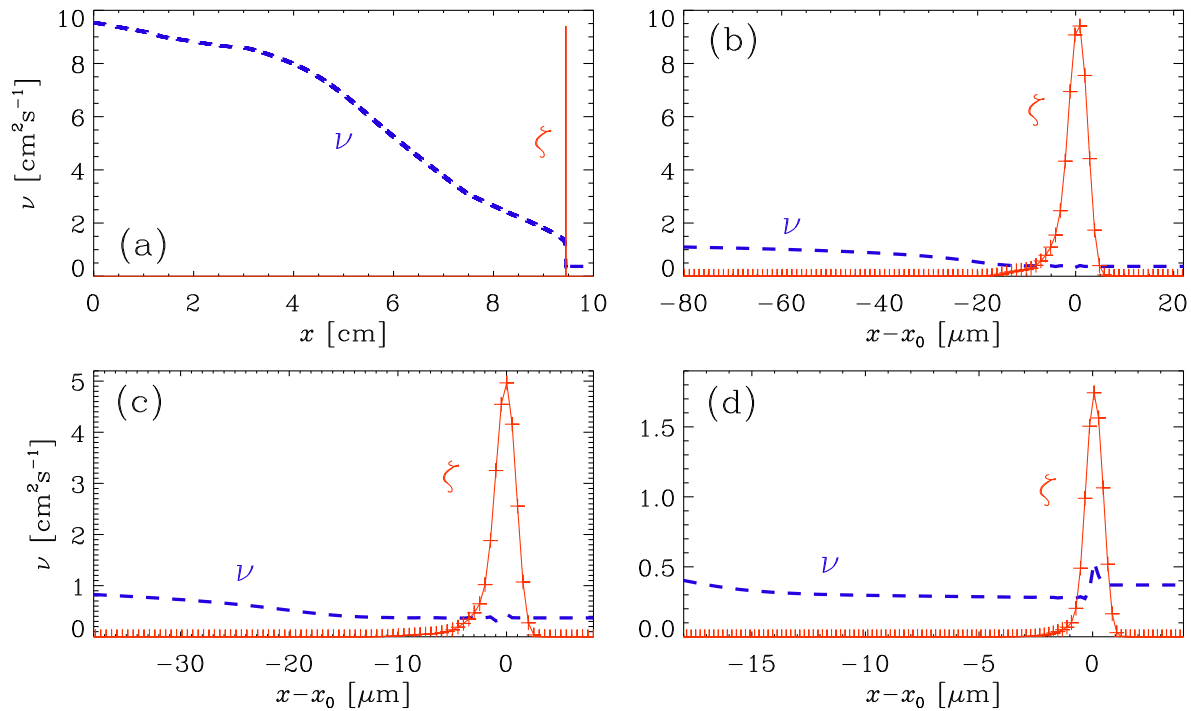


Figure 3. Comparison of the profiles of viscosity (ν , blue dashed lines) and shock viscosity (ζ , red lines with mesh points being marked with plus signs) for (a) $\delta x = 1 \mu\text{m}$ showing the full x range from 0 to 10 cm. (b)–(d) show only the close proximity of the shock at x_0 for (b) $\delta x = 1 \mu\text{m}$, (c) $\delta x = 0.5 \mu\text{m}$, and (d) $\delta x = 0.2 \mu\text{m}$, at $t = 42 \mu\text{s}$.

3.3. Dependence on C_{shock}

Next, we investigate the dependence of our solutions on the value of C_{shock} . In figure 4 we show pressure profiles for different values of C_{shock} at resolutions of $\delta x = 1 \mu\text{m}$ and $0.5 \mu\text{m}$. For $C_{\text{shock}} \leq 1.4$, the pressure profiles still show wiggles at the position of the pressure maximum, but the wiggles are smaller and more localised at the higher resolution of $0.5 \mu\text{m}$. For $C_{\text{shock}} = 1.4$, however, the wiggles are nearly completely negligible at a resolutions of $0.5 \mu\text{m}$, but the pressure profile has also changed in that case and has now a short flank with a negative slope just behind the shock, that is, to its left. For $C_{\text{shock}} = 1.5$, TD is only found in the case with $\delta x = 1 \mu\text{m}$, but not with $\delta x = 0.5 \mu\text{m}$.

In figure 5, we show a larger portion of the wake behind the pressure front, where we see the occurrence of another type of long-wavelength oscillation, when C_{shock} is larger than 0.8. Those waves are similar for both the higher and lower resolution runs, but could also be a feature of having under-resolved the solution at earlier times that are not shown here.

3.4. Speeds of pressure and reaction fronts

Finally, we show in figure 6 the time dependence of the positions and speeds of the pressure and spontaneous reaction fronts. In practice, the speeds U_i (with $i = p$ for pressure and $i = sr$ for spontaneous reaction wave) are computed by time differentiation of the position x_i , which is obtained from the volume where the pressure or the reactant are above a certain threshold. Specifically, we compute

$$U_p = \frac{dx_p}{dt} = -\frac{d}{dt} \int_0^{x_{\text{max}}} \max(p_{\text{crit}} - p, 0) / (p_{\text{crit}} - p_0) dx, \quad (24)$$

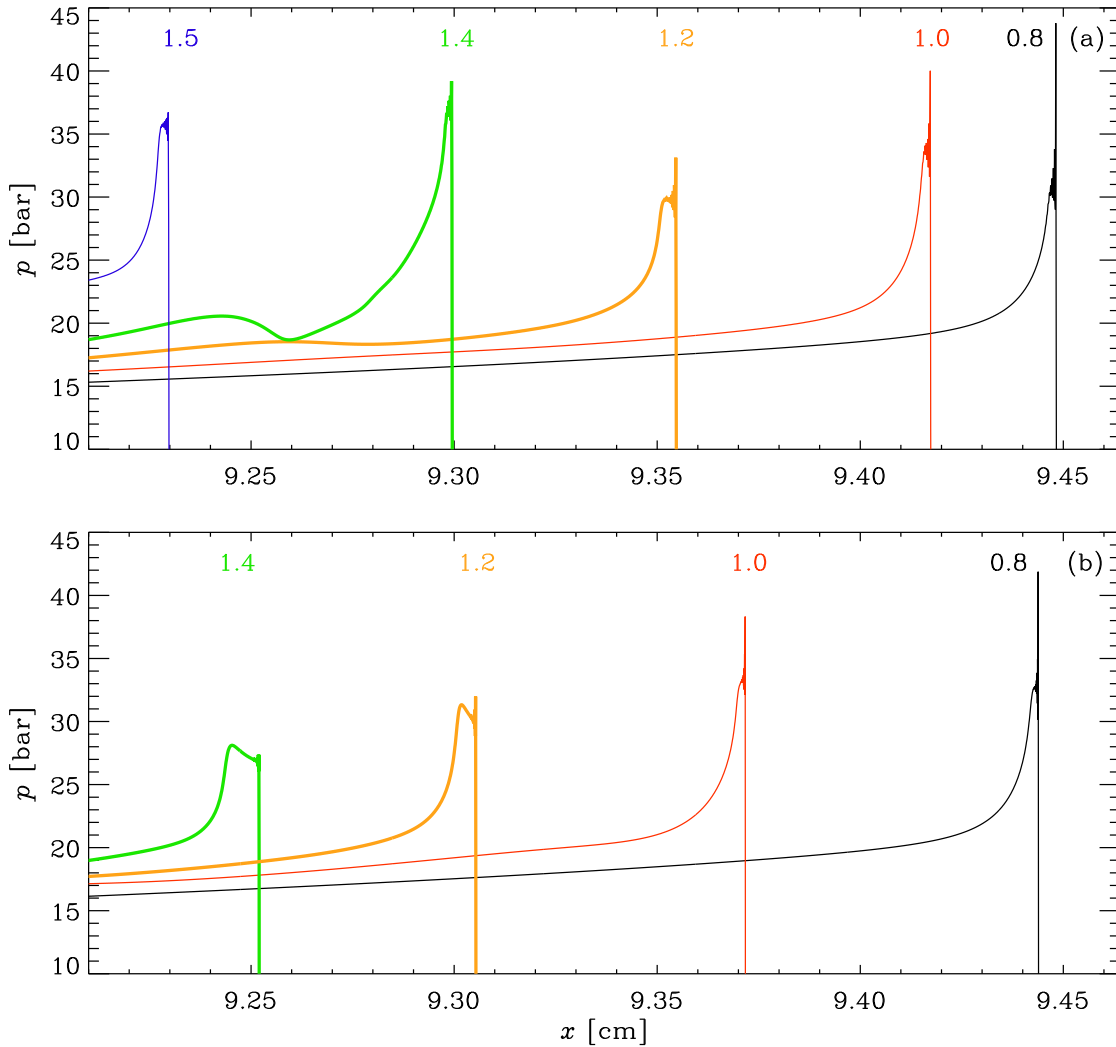


Figure 4. Comparison of pressure profiles for $C_{\text{shock}} = 0.8$ (black), 1.0 (red), 1.2 (orange), 1.4 (green), and 1.5 (blue), for $\delta x = 1 \mu\text{m}$ (top) and $0.5 \mu\text{m}$ (bottom). Note that for $C_{\text{shock}} = 1.5$ and $\delta x = 0.5 \mu\text{m}$, no TD develops.

where we have used $p_{\text{crit}} = 1.020$ bar as threshold pressure and $p_0 = 1.013$ bar is still the same background pressure as in equation (21). The spontaneous reaction speed is based on the amount of water produced, i.e.,

$$U_{\text{sp}} = \frac{dx_{\text{sp}}}{dt} = -\frac{d}{dt} \int_0^{x_{\text{max}}} \max(1 - Y_k/Y_{k0}, 0) dx, \quad (25)$$

where $k = \text{H}_2\text{O}$ and $Y_{k0} = 0.3$ is half the value of $Y_k \approx 0.6$ after H_2 has reacted with O_2 . The final values of the two speeds are $U_p = 3.06 \text{ km s}^{-1}$ and $U_{\text{sp}} = 3.01 \text{ km s}^{-1}$. These values are close to the empirically determined value of 3.0 km s^{-1} , which is only known to within about 1% accuracy and therefore compatible with our results.

According to equation (19), the velocity of the spontaneous reaction wave decreases in the beginning, since $U_{\text{sp}} \propto (d\tau_{\text{ind}}/dT)^{-1}$. It reaches a minimum somewhere near the crossover temperature $T_{\text{cr}} \approx 1000$ K (for the present mixture of H_2 and O_2) for the steepest gradient capable of initiating detonation which corresponds to the transition from the endothermal to the exothermal stage of the reaction. In our case, the gradient is rather shallower, so the minimum of the velocity is reached earlier.

After reaching the minimum velocity, the speed of the spontaneous reaction wave increases

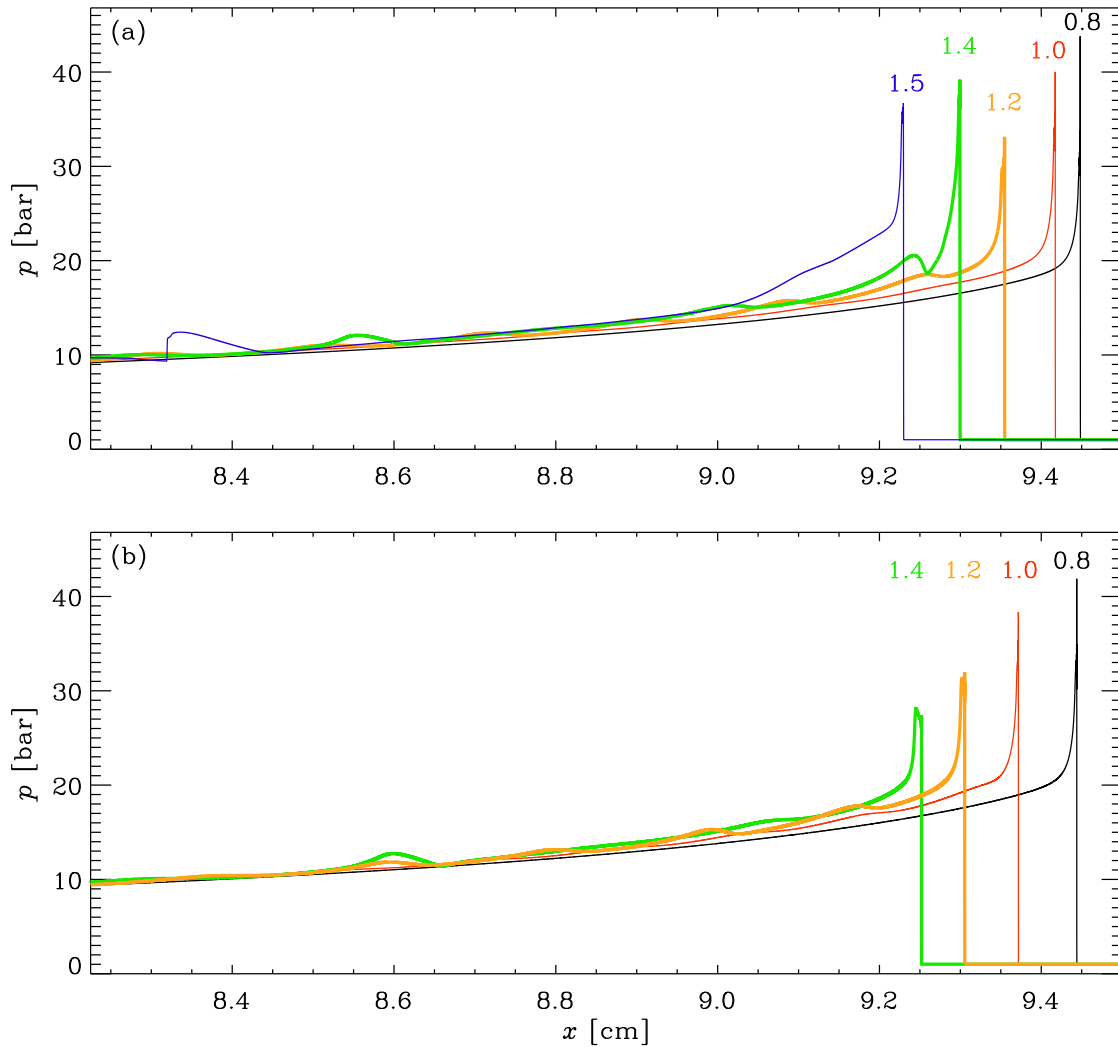


Figure 5. Similar to figure 4, but showing also the wake of the pressure front. Note the waves in the simulations with $C_{\text{shock}} > 0.8$ (see the blue, green, orange, and red lines).

due to energy release in the reaction. To accomplish coupling between the spontaneous reaction wave and the pressure wave, it is necessary (but not sufficient) that $U_{\text{sp}} > U_{\text{p}}$ after the point where U_{sp} is minimum, which is the case during the interval $12 \mu\text{s} \leq t \leq 19 \mu\text{s}$. For $t > 19 \mu\text{s}$, the coupling between the reaction wave and the shock wave is developing until detonation is reached at $t \approx 38 \mu\text{s}$. Note also that U_{sp} is now slightly less than U_{p} , but this is natural because the reaction happens always slightly behind the leading shock. In fact, at late times, hardly any difference between x_{p} and x_{sp} can be seen; see figure 6(a). This is compatible with the experimental value of the detonation; see Kuznetsov *et al.* (2005).

4. Conclusions

Using high-resolution simulations of detonation initiated by an initial temperature gradient in a hydrogen–oxygen mixture, we have shown that the transition to and properties of detonation can successfully be modelled for intermediate values of the shock viscosity parameter. The numerical error, as determined by comparing with an empirical fit to the pressure peak in the final stage of TD, is found to decrease like $\delta x^{1.4}$ with decreasing mesh size. The shock

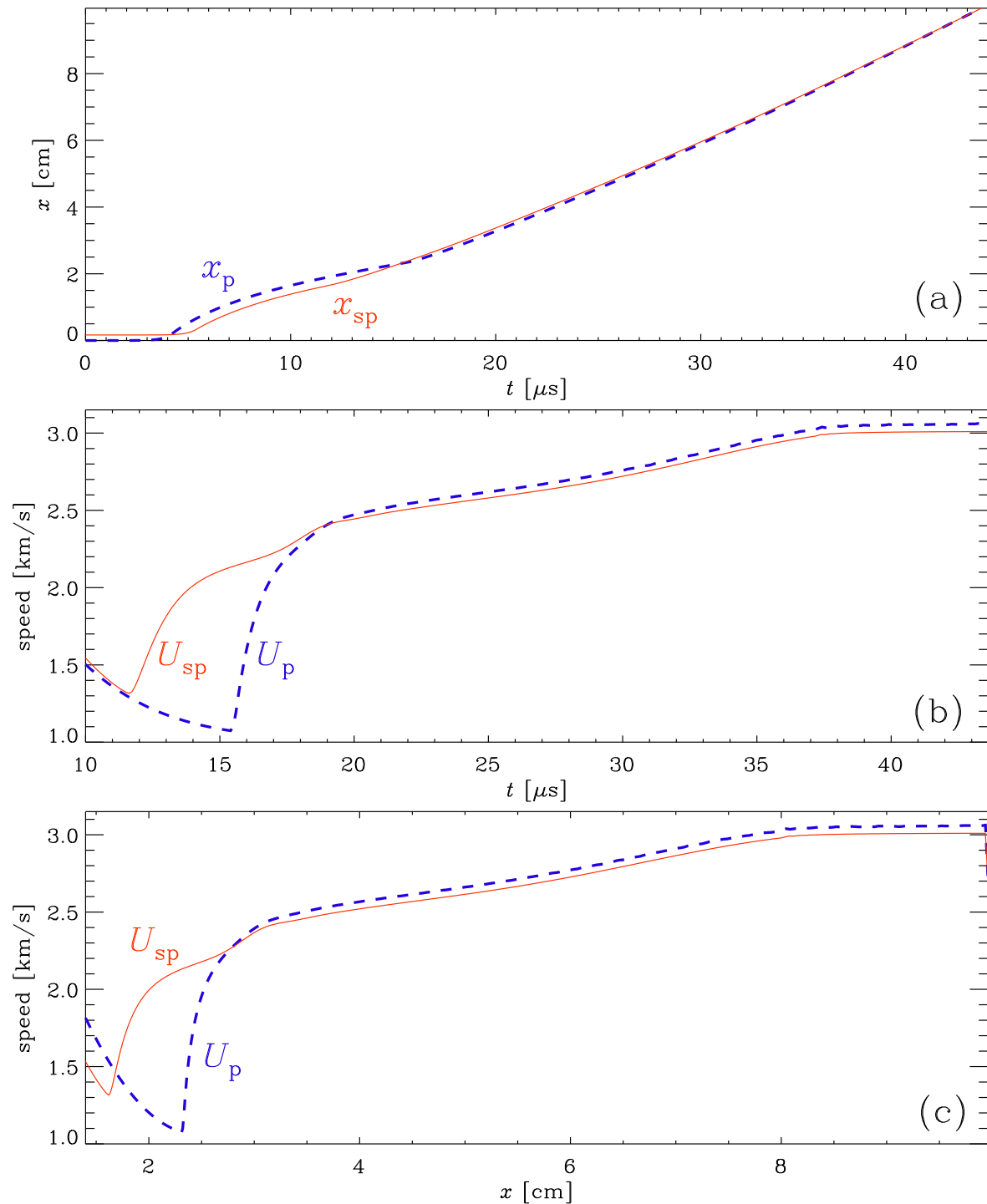


Figure 6. Front positions and speeds for $\delta x = 0.5 \mu\text{m}$ and $C_{\text{shock}} = 0.8$. (a) $x_{\text{sp}}(t)$ (red solid line) and $x_{\text{p}}(t)$ (blue dashed line), (b) $U_{\text{sp}}(t)$ (red solid line) and $U_{\text{p}}(t)$ (blue dashed line), and (c) $U_{\text{sp}}(x)$ (red solid line) and $U_{\text{p}}(x)$ (blue dashed line).

viscosity has non-vanishing values only in the immediate proximity of the shock and reaches there still values of about four times the molecular value in our highest resolution simulation. Unfortunately, the position of the shock still depends on the value of C_{shock} of around 3 km s^{-1} . Nevertheless, the shock speed reaches the expected value in the final stage of TD.

It remains unsatisfactory that even at the largest resolution of half a million mesh points in

just the x direction, we are still unable to avoid the use of a shock viscosity. This is because the shock is so strong and the molecular viscosity still too small by comparison. Furthermore, we have been unable to demonstrate that the use of a small amount of shock viscosity does not affect the details of the shock position or even the detailed shape of the shock profile. We can therefore not be completely sure that TD will still be recovered at even higher resolution, which has not yet been possible to simulate. A reason for the current limitation is that our code is optimised to work for three-dimensional problems. It is therefore conceivable that a significant speed-up could be achieved by optimising the code for one-dimensional problems. In that case it would also be rather straightforward to use an adaptive mesh, which could make the calculations significantly more economic.

Another possible avenue for future research is to solve the governing equations in conservative form so that mass, momentum, and energy are conserved to machine precision. A difficulty here is the presence of source terms in the equations for the mass fractions of the individual species. Comparison with the WENO scheme, which does use a conservative formalism, is already in progress. Unfortunately, the WENO scheme is computationally demanding and it is difficult to reach resolutions comparable to what has been done with the PENCIL CODE. (Its typical performance is $0.05 \mu\text{s}$ wall clock time per step and mesh point with 2048 processors on a Cray XC40 with 2.3 GHz Intel cores.) Moreover, in our preliminary investigations, it proved difficult to recover TD at high resolution. On the other hand, of course, we know from experiments that TD does occur. Thus, assuming that our equations are physically correct, as stated, there should be no doubt that any failure to recover TD must be regarded as a numerical artifact.

Yet another approach is to isolate the essence of the problem in a simpler single reaction model. One must then also use an idealised viscosity and a simplified equation of state. Those modifications could enable us to perform simulations at much higher resolution so that it is possible to focus on the purely numerical aspect of using a shock viscosity in this problem.

Acknowledgements

This research was supported in part by the National Natural Science Foundation of China (grant 11732003), the Beijing Natural Science Foundation (grant 8182050), the National Science Foundation under the Astronomy and Astrophysics Grants Program (grant 1615100), and the University of Colorado through its support of the George Ellery Hale visiting faculty appointment. Simulations presented in this work have been performed with computing resources provided by the Swedish National Allocations Committee at the Center for Parallel Computers at the Royal Institute of Technology in Stockholm.

References

- Babkovskaia, N., Haugen, N.E.L. and Brandenburg, A., A high-order public domain code for direct numerical simulations of turbulent combustion. *J. Comp. Phys.*, 2011, **230**, 1–12.
- Bartenev, A. and Gelfand, B., Spontaneous initiation of detonations. *Progress in Energy and Combustion Science*, 2000, **26**, 29–55.
- Coffee, T.P. and Heimerl, J.M., Transport algorithms for premixed, laminar steady-state flames. *Combustion and Flame*, 1981, **43**, 273–289.
- Evlampiev, A., *Numerical combustion modeling for complex reaction systems*, Vol. 68, 2007 (Eindhoven Techn. Univ., Eindhoven).
- He, L., Theoretical determination of the critical conditions for the direct initiation of detonations in hydrogen-oxygen mixtures. *Combustion and Flame*, 1996, **104**, 401–418.
- He, L. and Clavin, P., Critical conditions for detonation initiation in cold gaseous mixtures by nonuniform hot pockets of reactive gases; in *Symposium (International) on Combustion*, Vol. 24, 1992, pp. 1861–1867.
- Jiang, G. and Shu, C., Efficient implementation of weighted ENO schemes. *J. Comp. Phys.*, 1996, **126**, 202–228.

- Kéromnès, A., Metcalfe, W.K., Heufer, K.A., Donohoe, N., Das, A.K., Sung, C.J., Herzler, J., Naumann, C., Griebel, P., Mathieu, O., Krejci, M.C., Petersen, E.L., Pitz, W.J. and Curran, H.J., An experimental and detailed chemical kinetic modeling study of hydrogen and syngas mixture oxidation at elevated pressures. *Combustion and Flame*, 2013, **160**, 995–1011.
- Khokhlov, A., Oran, E. and J. W., A theory of deflagration-to-detonation transition in unconfined flames. *Combustion and Flame*, 1997, **108**, 503–517.
- Kurtz, M.D. and Regele, J.D., Acoustic timescale characterisation of a one-dimensional model hot spot. *Combustion Theory and Modelling*, 2014, **18**, 532–551.
- Kuznetsov, M., Alekseev, V., Matsukov, I. and Dorofeev, S., DDT in a smooth tube filled with a hydrogen oxygen mixture. *Shock Waves*, 2005, **14**, 205–215.
- Lee, J. and Moen, I., The Mechanisms of Transition from Deflagration to Detonation in Vapor Cloud Explosions. *Progress in Energy and Combustion Science*, 1980, **6**, 359–389.
- Liberman, M.A., Kiverin, A.D. and Ivanov, M.F., On detonation initiation by a temperature gradient for a detailed chemical reaction models. *Phys. Lett. A*, 2011, **375**, 1803–1808.
- Liberman, M.A., Wang, C., Qian, C. and Liu, J., Influence of chemical kinetics on spontaneous waves and detonation initiation in highly reactive and low reactive mixtures. *Combustion Theory and Modelling*, DOI:10.1080/13647830.2018.1551578, 2018, pp. 1–29.
- Liberman, M.A., Kiverin, A. and Ivanov, M., Regimes of chemical reaction waves initiated by nonuniform initial conditions for detailed chemical reaction models. *Phys. Rev. E*, 2012, **85**, 056312.
- Lo, S.C., Blaisdely, G.A. and Lyrantzisz, A.S., High-order shock capturing schemes for turbulence calculations. *45th AIAA Aerospace Sciences Meeting and Exhibit, January 8-11, 2007*, 2007, pp. 1–18.
- Mourits, M.M. and Rummens, F.H.A., A critical evaluation of Lennard-Jones and Stockmayer potential parameters and of some correlation methods. *Can. J. Chem.*, 1977, **55**, 3007–3020.
- Poinsot, T. and Veynante, D., *Theoretical and numerical combustion*, 2005 (RT Edwards, Inc.).
- von Neumann, J. and Richtmyer, R.D., A method for the numerical calculation of hydrodynamic shocks. *J. Appl. Phys.*, 1950, **21**, 232–237.
- Wang, C., Qian, C., Liu, J. and Liberman, M.A., Influence of chemical kinetics on detonation initiating by temperature gradients in methane/air. *Combustion and Flame*, 2018, **197**, 400–415.
- Wilke, C.R., A viscosity equation for gas mixtures. *J. Comp. Phys.*, 1950, **18**, 517–519.
- Zeldovich, Y.B., Regime classification of an exothermic reaction with nonuniform initial conditions. *Combustion and Flame*, 1980, **39**, 211–214.
- Zeldovich, Y.B., Gelfand, B., Tsyganov, S., Frolov, S. and Polenov, A., Concentration and temperature nonuniformities of combustible mixtures as reason for pressure waves generation. *Dynamics of explosions*, 1988, **114**, 99.
- Zeldovich, Y., Librovich, V., Makhviladze, G. and Sivashinsky, G., On the development of detonation in a non-uniformly preheated gas. *Acta Astron.*, 1970, **15**, 313–321.